第 48 卷 第 3 期/2021 年 2 月/中国激光 研究论文

中国激光

免偏振敏感消色差超构镜设计研究

梁瑜[1]，徐媛媛[1*]，邹阳[2]，薛双双[1]，廖景荣[3]，潘文雁[1]，王亚伟[1]

[1]江苏大学物理与电子工程学院，江苏 镇江 212013；

[2]江苏大学京江学院，江苏 镇江 212013；

[3]江苏大学机械工程学院，江苏 镇江 212013

摘要 超构透镜作为一种灵活调控空间光场相位、振幅及偏振的有效选择，在超分显微成像中受到了广泛的关注。为了提高多波长显微成像的分辨率，解决传统光学系统结构厚重、设计复杂等问题，基于相位补偿理论，运用传输相位法以及粒子群优化算法，设计了一种基于二氧化钛纳米单元柱的反射式消色差超构透镜，在 500～550 nm 之间实现了恒定聚焦，且该透镜具有偏振不敏感的特性。与数值孔径相同但有色散的超构透镜的对比结果有效证实了该超构透镜的消色差功能。所设计的透镜可应用于多波长显微成像系统中并提高成像的分辨率。此外，该消色差透镜在数码相机和光学仪器等领域中也有较好的应用价值。

关键词 光学设计；光学材料；超构透镜；消色差透镜；免偏振敏感；多波长；显微成像

中图分类号 O436 **文献标志码** A **doi**：10.3788/CJL202148.0303001

1 引 言

传统的光学显微成像方式是利用透过样本后的光强度分布来获取目标样本的显微成像，但成像结果的对比度较低且分辨率不高。1873 年，德国物理学家发现光学成像存在衍射极限现象，即光束在离开物体表面时，携带有细微信息的倏逝波在近场呈指数迅速衰减，因此成像质量受到影响。普通光学显微镜能分辨的最小尺寸为半个波长。同时，受限于传统光学的调制机理，光学系统的高度集成化仍然较难[1-3]。超构透镜作为一种新兴左手材料，可放大倏逝波并对传统透镜丢失的细微信息进行恢复，具有小型化及可对相位、振幅和偏振进行灵活调控等优势[4-8]，使得越来越多的高度紧凑且高效率的设备得以实现[9-12]，成像更加完美。2000 年，英国物理学家 Pendry[13] 利用周期性排列的金属条，使具有负折射现象的左手材料得以实现。2013 年，美国 Ni 等[14] 利用 V 型纳米棒结构，在可见光波段设计了具有聚焦功能的超构透镜。然而，不同频率入射光通过介质材料后会产生色散现象，这极大影响了宽波段范围内光学系统的成像效果。2015 年，Khorasaninejad 等[15] 利用硅介质长条结构，设计了近红外波长为 1300，1550，1800 nm 时可实现消色差聚焦的超构透镜。2018 年，Chen 等[16] 利用各向异性结构，在可见光波段 470～670 nm 范围内实现了消色差聚焦超构透镜，但该透镜具有一定的偏振敏感性。几何相位型超表面受光束偏振态的影响，单元结构仅在特定偏振方向发生变化且产生对应的相位延迟，而偏振片的加入会导致入射光能量大大减小，使光学器件的能量利用率偏低[17-18]。已报道的具有宽带消色差能力的超构透镜可应用于可见光及近红外光中，但是大部分都具有偏振敏感性[19]，仅能聚焦给定的圆偏振光。目前，研究者利用各向同性或各向异性纳米单元柱等[20-22]，在可见光谱和近红外光谱中克服了偏振不敏感性[23-26]，已设计出具有高效率与高数值孔径等优势[27-30]的超构透镜。但是可实现偏振不敏感且消色差的超构透镜依然较少[31-32]。在超构透镜清晰成像时，引入的偏振片会

收稿日期：2020-08-19；**修回日期**：2020-09-13；**录用日期**：2020-09-27

基金项目：国家自然科学基金(11874184)、中国博士后基金(2019M651769)、江苏省博士后基金(2018K032A)、江苏大学青年英才培训(41119007)

* **E-mail**：yuanyuanxulark@126.com

导致器件能量利用率偏低。为了解决这一问题，本文选用各向同性的二氧化钛(TiO_2)纳米单元柱，设计了偏振不敏感消色差超构透镜，使器件的能量利用率有所提高，设计便捷且相位覆盖率大，在入射光波长 500～550 nm 范围内保持了恒定焦距 $f=450\ \mu m$，有效消除了宽波长域色差。本文同时设计了数值孔径相同的有色散超构透镜并进行了对比。

2 基本原理

由于透镜的消色差作用，光束通过超构透镜后聚焦到一点，如图 1 所示。

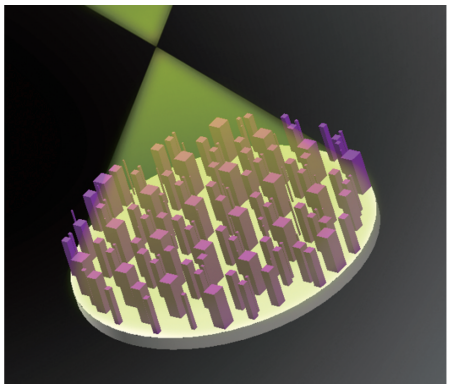

图 1 超构透镜聚焦示意图

Fig. 1 Schematic of focusing by metalens

在本文设计的消色差聚焦超构透镜中，每一点处所需要的基础相位与该点所在的坐标位置满足

$$\varphi(x,y,\lambda)=2k\pi+\frac{2\pi}{\lambda}\sqrt{x^2+y^2+f^2}+C,\quad(1)$$

式中：$\varphi(x,y,\lambda)$为超构透镜的亚波长单元结构引起的相位突变；λ 是入射光波长；k 为波数；f 为设计的焦距；(x,y)为超构透镜上每一点的坐标；C 为调节波面的附加常数相位。通过(1)式得到超构透镜的基础相位分布：

$$\varphi(r,\omega)=\varphi(r,\omega_0)+\frac{\partial\varphi}{\partial\omega}\Big|_{\omega=\omega_0}(\omega-\omega_0)+\frac{\partial^2\varphi}{2\partial\omega^2}\Big|_{\omega=\omega_0}(\omega-\omega_0)^2+\cdots,\quad(2)$$

式中：$\varphi(r,\omega_0)$为 $r=\sqrt{x^2+y^2}$ 处所需实现的相位；ω_0 为中心波长频率；$\frac{\partial\varphi}{\partial\omega}\Big|_{\omega=\omega_0}(\omega-\omega_0)$为群延迟；$\frac{\partial^2\varphi}{2\partial\omega}\Big|_{\omega=\omega_0}(\omega-\omega_0)^2$ 为群延迟色散。将入射光视为波包，向焦点处发送入射波包，其中一阶导数项和高阶导数项确保了入射波包在时域上同时到达焦点，因此要找到可满足该条件并能有效调控入射光的纳米结构。大部分利用几何相位进行设计的超构透镜，都将基础相位与调制相位分离，但这种方法设计出的超构透镜大多数都具有偏振敏感性，仅能聚焦特定的圆偏振入射光。本文利用传输相位法对消色差超构透镜进行设计，使线偏振光和圆偏振光都可入射，有效实现了偏振不敏感。在传统的折射透镜中，由于相位易受材料的影响，一般都选取如二氧化硅等低色散材料，当光透过不同厚度的透镜时，通过调节光束的偏折角可实现连续相位，达到色差校正的效果。本文在超构透镜的设计中，通过设计不同宽度不同排列方式的亚波长单元柱，实现了对电磁波的灵活调控，避免了传统透镜功能单一且不易集成的缺陷，有效实现了消色差功能。在此过程中，亚波长纳米单元柱的设计与排列是影响超构透镜功能的最重要部分，本文选取高度较大且宽度较小的二氧化钛纳米单元柱。为了最大化提高相位覆盖率，需要对纳米柱的参数进行优化，包含纳米柱形状的选取、宽度、高度及相邻纳米柱中心到中心的距离，由于单元柱高度越大，相位覆盖率越大，最终选取了高度为 600 nm 的正方形单元柱。首先，正方形截面具有最大化的 0～1 填充因子范围，保障了大相位覆盖率，且可保证偏振不敏感。其次，对纳米柱的宽度进行选取，受超构透镜制造工艺的限制，最小可实现的宽度为 80 nm，最大宽度为相邻纳米柱的中心距，这个选取遵循奈奎斯特采样准则，透过的光束信息不会丢失，聚焦效率不受影响。利用 CST 电磁仿真软件(CST Microwave Studio)对二氧化钛纳米单元柱进行参数扫描，得到所需相位对应的纳米单元柱宽度。此外，为了激发不同色散的导模发生共振，纳米单元柱的周期应大于透过的所有波长带宽，同时小于自由空间中的入射光波长，以抑制更高阶的衍射，因此选取单元柱周期为 $U=400$ nm。

在超构透镜的纳米单元柱确定后，针对消色差所需的相位分布进行单元柱的排列。对于一般有色差的超构透镜，不同波长处的相位积累是不同的，因此不同波长的入射光无法聚焦到同一点。为了更好实现消色差，使不同波长的入射光到达焦点的相位间隔最小，将 500～550 nm 区间离散为 6 个等间距的波长，并使超构透镜的焦距 $f=450\ \mu m$ 和直径 $D=12\ \mu m$；计算出每个波长所需的相位，利用粒子群优化(Particle swarm optimization)算法找出具有调节作用的常数 C，使所需的理想相位与实际相位之间的差值 $\Delta\varphi$ 最小，即得到准确的相位分布结果。由于同一波长光束在超构透镜不同纳米单元柱上的相位值是不同

的，且不同波长光束在超构透镜同一纳米单元柱上的相位值也是不相同的，因此不同像素点在不同波长下的相位差也是不相同的，并与坐标位置等没有确切关系。为了在一定带宽内实现消色差聚焦效果，利用 CST 电磁仿真软件，对本文选取的正方形纳米单元柱进行固定步长的参数扫描，得到了不同宽度正方形纳米单元柱的反射相位，然后利用粒子群优化算法，在数据库中选择出合适的结构，以匹配每个像素点处的理想相位值。粒子群优化算法流程如图 2 所示。

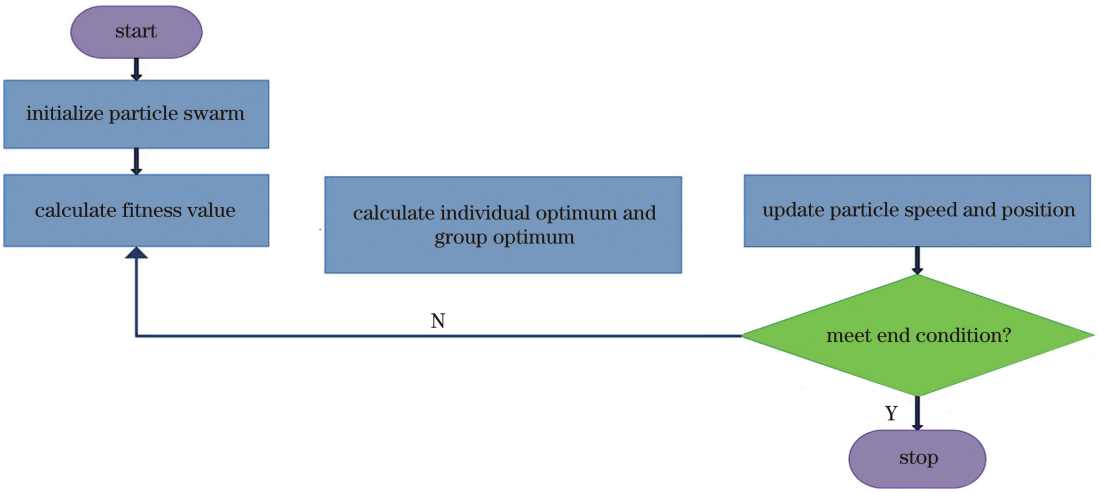

图 2 粒子群优化算法流程

Fig. 2 Flow chart of particle swarm optimization algorithm

3 模拟仿真和结果分析

由于传统透镜所用的二氧化硅的色散系数相对较低，可以通过多个透镜级联的方式直接纠正色差。而基于超构表面的衍射透镜常通过波导效应获取所需相位，因此对超构透镜不同位置处的纳米单元柱进行排布，从而对整体结构进行排布。首先对纳米单元柱进行参数扫描以构建单元库，运用基于有限积分法(Finite Integration)的三维 CST 电磁仿真软件展开参数扫描，并基于 MATLAB 采用粒子群优化算法找出附加常数相位，使超构透镜结构中每个单元柱实际所需相位与单元库中单元柱相位之间的差距最小。本文选取高度为 $h=600$ nm、单元周期为 $U=400$ nm 的二氧化钛正方形纳米单元柱，在入射光波段 500～550 nm 之间进行参数扫描，二氧化钛纳米单元柱的介电系数为 90，边界条件在 x 和 y 方向都设置为单元边界，在 z 方向都设置为辐射边界，辐射边界与开放边界类似但增加了额外空间以计算远场辐射的特性。针对正方形单元柱宽度的固定改变进行参数扫描，步进为 2，得到超构透镜所需的不同反射相位。图 3 是入射光波长为 500，530，550 nm 时，正方形纳米单元柱宽度在 0～400 nm 范围内对应的相位，相位可覆盖 0～2π，且不同波长下相位随着纳米柱宽度的变化呈线性。受超构透镜制备工艺的限制，实际选取的纳米柱最小宽度为 80 nm。

通过参数扫描获取不同宽度纳米单元柱的相位

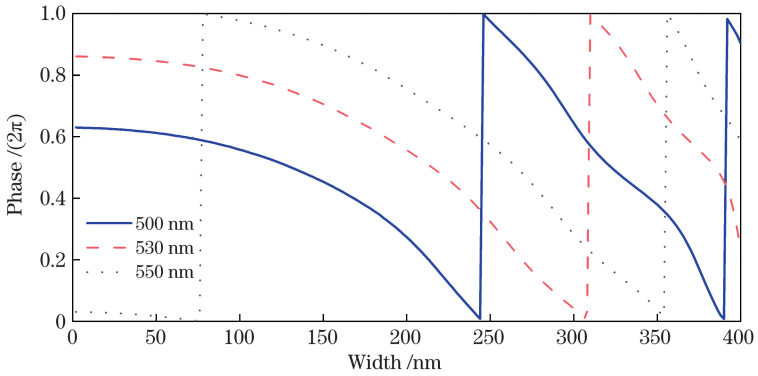

图 3 不同波长下不同宽度单元柱的相位

Fig. 3 Phase of unit column under different widths and wavelengths

后，为了实现超构透镜的消色差效果，需使不同波长光束在相同宽度纳米柱处的相位差值尽量小，因此选用粒子群优化算法求解附加常数相位 C。选取 520 nm 为中心波长，使波长分别为 500，510，530，540，550 nm 的光束与波长为 520 nm 的光束的相位差值最小，最终获得最优附加常数相位即 C 取值为 260 nm。根据聚焦原理可知，为了使超构透镜对相同焦距处的不同波长入射光的相位调制一致，衍射透镜的实际焦距应满足

$$f(\lambda)=\frac{f_0\lambda_0}{\lambda},\tag{3}$$

式中：λ_0 和 f_0 分别是设计波段的波长和焦距。当入射波长与超构透镜设计波长不同时，会产生焦距偏移，导致聚焦效率下降，且成像系统的分辨率减小。因此，本文将 500～550 nm 区间离散为 6 个等间距的波长，将不同波长处的标准聚焦相位剖面与优化后的相位剖面进行对比，如图 4 所示，发现在未用粒子群优化算法时，相位偏移明显，不同波长的相位分布有较大差距，聚焦效率过低且有明显色差。由图 4 还可以发现，在不同波长处，消色差超构透镜中心处实际所需的相位各不相同。

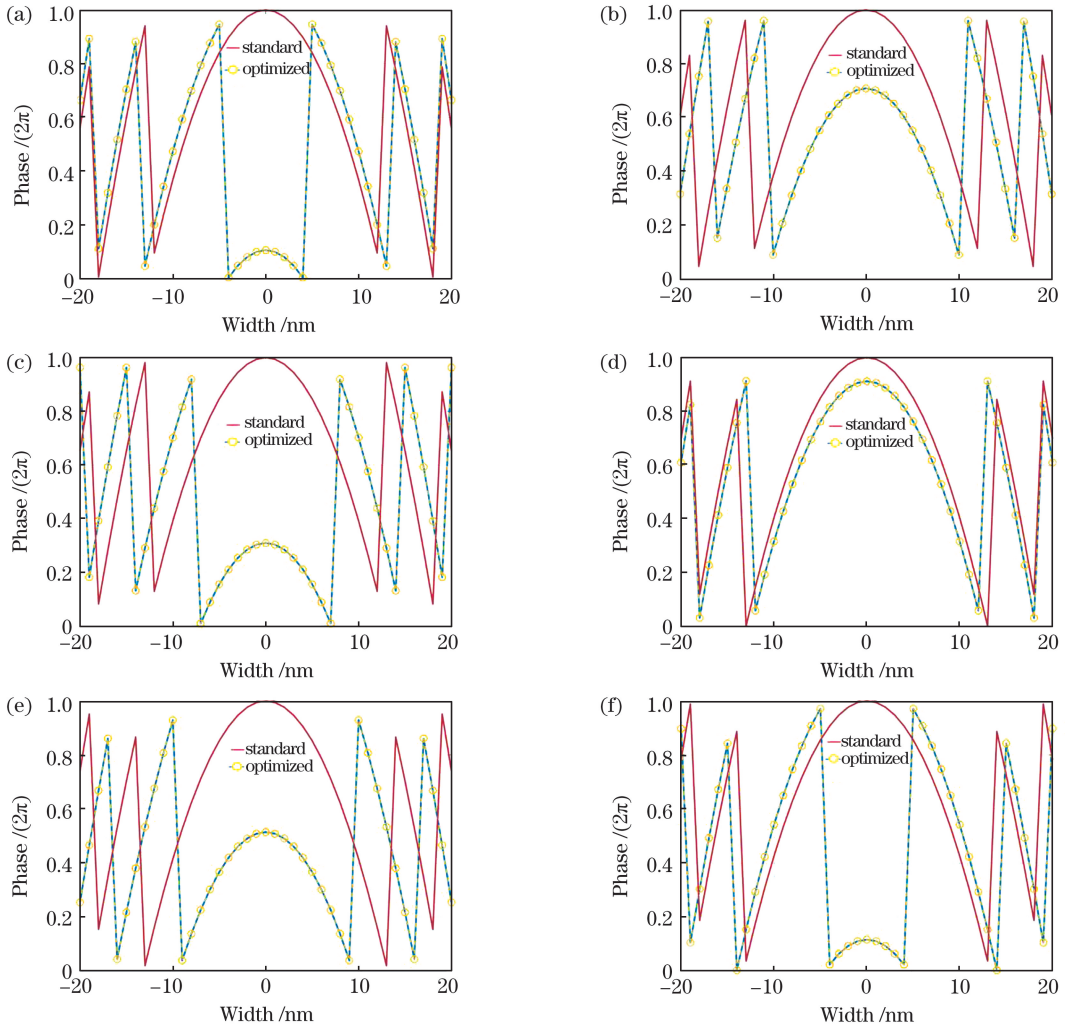

图 4　不同波长处标准聚焦相位剖面与优化后的相位剖面对比。(a) 500 nm；(b) 510 nm；(c) 520 nm；(d) 530 nm；(e) 540 nm；(f) 550 nm

Fig. 4　Comparison between standard focus phase profile and optimized phase profile at different wavelengths. (a) 500 nm; (b) 510 nm; (c) 520 nm; (d) 530 nm; (e) 540 nm; (f) 550 nm

所设计的消色差超构透镜得到最优相位分布后，对超构透镜不同位置处的纳米单元柱进行排布。图 5(a)为超构透镜整体结构的俯视图。图 5(b)为本文所设计的超构透镜的纳米单元柱，单元柱的横截面是宽度为 w 的正方形，通过调节宽度 w 对反射相位进行控制。衬底是厚度为 $b=150$ nm 的二氧化硅，中间层是厚度为 $a=100$ nm 的反射铝板。图 5(c)为正方形纳米单元柱的俯视图，所用的二氧

化钛纳米单元柱的周期 $U=400$ nm。

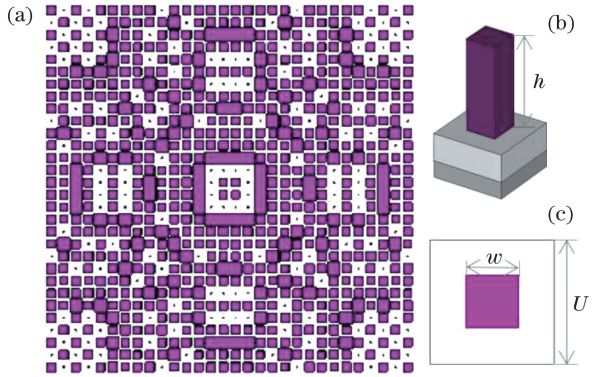

图 5　超构透镜纳米单元柱与结构排布。(a)超构透镜结构的俯视图;(b)纳米单元柱;(c)纳米单元柱的俯视图

Fig. 5　Unit nanopillar and structural arrangement of metalens. (a) Top view of metalens structure; (b) unit nanopillar; (c) top view of unit nanopillar

对本文所设计的免偏振敏感消色差超构透镜结构完整排布后,当焦距与直径一定时,所设计的超构透镜的数值孔径为

$$NA(\lambda)=D/\left[2\sqrt{f^2(\lambda)+D^2/4}\right]。\tag{4}$$

为了验证本文所设计的超构透镜的消色差性能,利用三维 CST 电磁仿真软件在时域求解器中进行模拟。在入射光波段 500～550 nm,具有相同焦距和数值孔径的消色差超构透镜和有色差超构透镜的焦距变化对比图如图 6 所示。不同波长光通过本文设计的消色差超构透镜后,聚焦在距离超构透镜 $z=450$ μm 处,实现了消色差效果,如图 6(a)所示。不同波长光通过本文设计的有色差超构透镜后,焦距随波长的增加而减小,如图 6(b)所示,虚线的位置对应于波长为 520 nm 光束的焦距。

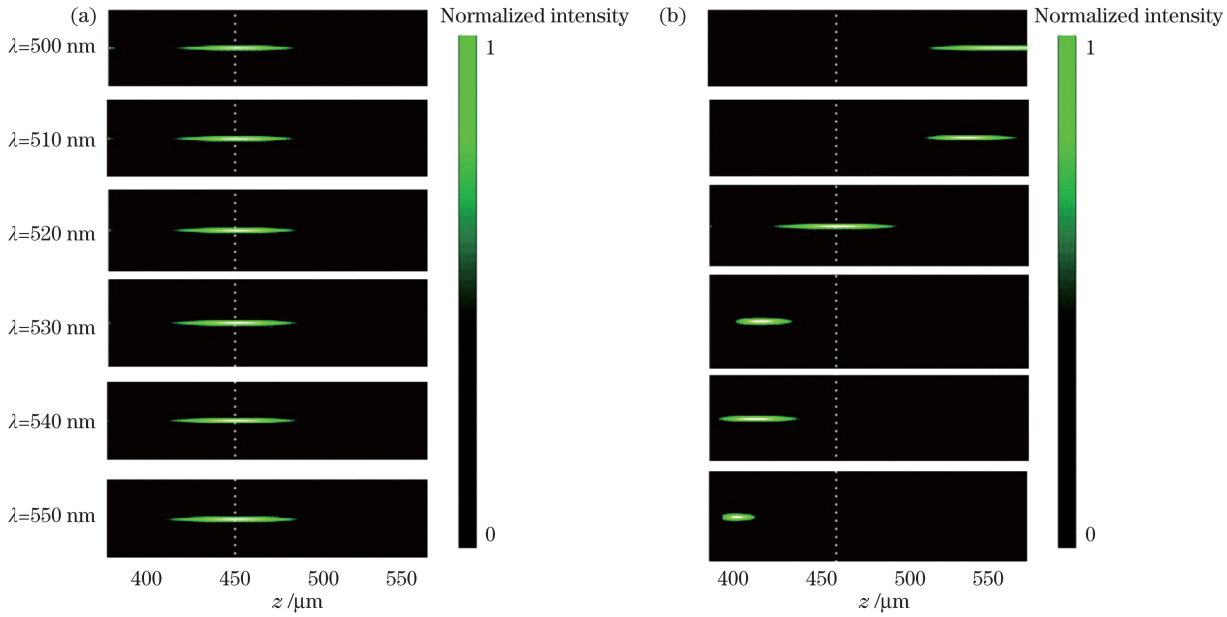

图 6　消色差超构透镜与有色散超构透镜的聚焦对比。(a)消色差;(b)有色差

Fig. 6　Focus comparison between achromatic metalens and chromatic metalens. (a) Achromatic; (b)chromatic

模拟仿真结果证明了本文所设计的消色差超构透镜的有效性,该超构透镜实现了入射光波长在 500～550 nm 之间的焦距恒定。超构透镜的焦距变化为

$$\eta=\frac{\max(f)-\min(f)}{\mathrm{mean}(f)}\times 100\%,\tag{5}$$

式中:η 为焦距变化;$\max(f)$ 为最大焦距;$\min(f)$ 为最小焦距;$\mathrm{mean}(f)$ 为中心波长焦距。本文所设计的超构透镜的焦距变化为 9.5%,进一步验证了本文消色差方法的有效性。

当入射光波长为 500～550 nm 时,以结构中心为原点,结构基面为 xoy 面,光束入射方向为 z 轴,对本文所设计的超构透镜在 xoy 平面上的反射率进行模拟,结果如图 7 所示,显示反射率在 xoy 平面上超过 90%。

为了避免偏振片的引入导致能量损失这一问题,本文所设计的消色差超构透镜具有偏振不敏感特性。在许多实际应用中,需要所设计的超构透镜不仅能在正入射的情况下具有偏正不敏感特性,还需要在不同入射角度下具有偏振不敏感的性能。选取正方形纳米单元柱作为功能单元,对其周期和占空比进行调控,使得横电(TE)模和横磁(TM)模具

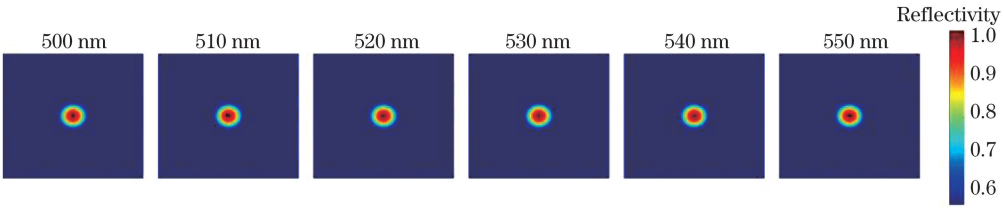

图 7 不同波长下 xoy 平面上的反射率

Fig. 7 Reflectivity of reflected beam in xoy plane under different wavelengths

有相同的耦合强度，从而实现偏振不敏感。线偏振光强度可看作是两个分量强度的总和，在线偏振光入射条件下，设定偏振角为 0～90°，以 9°为步进，利用三维 CST 电磁仿真软件对单个纳米柱进行参数扫描。在不同入射角下，不同偏振态入射光的两个分量的反射相位和振幅与设计值相同，相同入射波长光的衍射效率也保持恒定，且随着波长的增大，衍射效率增大，如图 8 所示。因此，本文所设计的超构透镜在不同偏振光下具有相同的波前，即偏振不敏感。而圆偏振光可看作是两个线偏振光的叠加，其振幅相同，偏振方向垂直，相位差为 π/2，其聚焦强度仍然为两个分量的叠加，因此本文所设计的超构透镜有效实现了消色差且具有偏振不敏感性能。

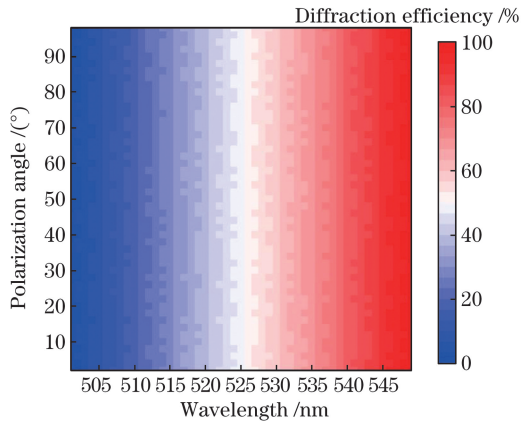

图 8 偏振入射光的衍射效率

Fig. 8 Diffraction efficiency of polarized incident light

4 结 论

基于传输相位理论，利用二氧化钛纳米材料设计了可见光下的反射式超构透镜。在入射光波长 500～550 nm 区间，该超构透镜成功消除了色差且具有偏振不敏感性能。设计了数值孔径相同且有色散的超构透镜，实现了传统衍射光学限制的突破。与其他基于几何相位理论的超构透镜相比，所设计的超构透镜使任何状态的线偏振光以及具有不同手性的圆偏振光都可入射，实现了消色差效果。与由各向异性纳米单元柱构成的超构透镜相比，所提设计方法更为简便。这种方法为其他消色差偏振不敏感超表面器件的设计提供了参考，设计的偏振不敏感且具有消色差的超构透镜在显微成像及光学仪器等领域中具有重要的应用价值。

参 考 文 献

[1] Wintz D, Genevet P, Ambrosio A, et al. Holographic metalens for switchable focusing of surface plasmons [J]. Nano Letters, 2015, 15(5): 3585-3589.

[2] Fu B Y, Zou X J, Li T, et al. Review: chromatic dispersion manipulation based on optical metasurfaces [J]. Journal of Harbin Institute of Technology (New Series), 2020, 27(3): 1-19.

[3] Cao C, Liao S, Liao Z Y, et al. Design of off-axis reflective optical system with large field-of-view based on freeform surfaces [J]. Acta Optica Sinica, 2020, 40(8): 0808001.
操超, 廖胜, 廖志远, 等. 基于自由曲面的大视场离轴反射光学系统设计[J]. 光学学报, 2020, 40(8): 0808001.

[4] Siddique R H, Mertens J, Hölscher H, et al. Scalable and controlled self-assembly of aluminum-based random plasmonic metasurfaces [J]. Light: Science & Applications, 2017, 6(7): e17015.

[5] Chen W T, Zhu A Y, Sisler J, et al. Broadband achromatic metasurface-refractive optics [J]. Nano Letters, 2018, 18(12): 7801-7808.

[6] Jahani S, Jacob Z. All-dielectric metamaterials [J]. Nature Nanotechnology, 2016, 11(1): 23-36.

[7] Li H, Yu J, Chen Z. Switchable broadband absorber/reflector with polarization-independent and incident angle-insensitive based on single-layer graphene [J]. Chinese Journal of Lasers, 2020, 47(8): 0803001.
李辉, 余江, 陈哲. 基于单层石墨烯的偏振无关和入射角度不敏感的可切换宽带吸收器/反射器[J]. 中国激光, 2020, 47(8): 0803001.

[8] Gu M M, Wang D W, Chen X L, et al. Research progress of silicon photonic polarization beam-splitting rotary devices [J]. Laser & Optoelectronics Progress, 57(17): 170002.
顾苗苗, 汪大伟, 陈晓铃, 等. 硅光子偏振分束旋转器

件研究进展[J]. 激光与光电子学进展, 2020, 57(17): 170002.

[9] Wang S M, Wu P C, Su V C, et al. Broadband achromatic optical metasurface devices[J]. Nature Communications, 2017, 8(1): 187.

[10] Cheng Q Q, Ma M L, Yu D, et al. Broadband achromatic metalens in terahertz regime[J]. Science Bulletin, 2019, 64(20): 1525-1531.

[11] Wintz D, Genevet P, Ambrosio A, et al. Holographic metalens for switchable focusing of surface plasmons[J]. Nano Letters, 2015, 15(5): 3585-3589.

[12] Zhu R, Tao C X, Yu Z, et al. Design and fabrication of a 248 nm near-linearly graded transmittance optical film[J]. Chinese Journal of Lasers, 2020, 47(6): 0603001.
朱瑞, 陶春先, 余振, 等. 248 nm 透过率线性渐变光学薄膜的设计与制备[J]. 中国激光, 2020, 47(6): 0603001.

[13] Pendry. Negative refraction makes a perfect lens[J]. Physical Review Letters, 2000, 85(18): 3966-3969.

[14] Ni X J, Ishii S, Kildishev A V, et al. Ultra-thin, planar, Babinet-inverted plasmonic metalenses[J]. Light: Science & Applications, 2013, 2(4): e72.

[15] Khorasaninejad M, Aieta F, Kanhaiya P, et al. Achromatic metasurface lens at telecommunication wavelengths[J]. Nano Letters, 2015, 15(8): 5358-5362.

[16] Chen W T, Zhu A Y, Sanjeev V, et al. A broadband achromatic metalens for focusing and imaging in the visible[J]. Nature Nanotechnology, 2018, 13(3): 220-226.

[17] Luo X G, Pu M B, Li X, et al. Broadband spin Hall effect of light in single nanoapertures[J]. Light: Science & Applications, 2017, 6(6): e16276.

[18] Maguid E, Yulevich I, Yannai M, et al. Multifunctional interleaved geometric-phase dielectric metasurfaces[J]. Light: Science & Applications, 2017, 6(8): e17027.

[19] Wang S M, Wu P C, Su V C, et al. A broadband achromatic metalens in the visible[J]. Nature Nanotechnology, 2018, 13(3): 227-232.

[20] Chen W T, Zhu A Y, Sisler J, et al. A broadband achromatic polarization-insensitive metalens consisting of anisotropic nanostructures[J]. Nature Communications, 2019, 10(1): 355.

[21] Lin D, Holsteen A L, Maguid E, et al. Polarization-independent metasurface lens employing the Pancharatnam-Berry phase[J]. Optics Express, 2018, 26(19): 24835-24842.

[22] Zhang X H, Li X, Jin J J, et al. Polarization-independent broadband meta-holograms via polarization-dependent nanoholes[J]. Nanoscale, 2018, 10(19): 9304-9310.

[23] Khorasaninejad M, Shi Z, Zhu A Y, et al. Achromatic metalens over 60 nm bandwidth in the visible and metalens with reverse chromatic dispersion[J]. Nano Letters, 2017, 17(3): 1819-1824.

[24] Shrestha S, Overvig A C, Lu M, et al. Broadband achromatic dielectric metalenses[J]. Light: Science & Applications, 2018, 7: 85.

[25] Wang E L, Shi L N, Niu J B, et al. Multichannel spatially nonhomogeneous focused vector vortex beams for quantum experiments[J]. Advanced Optical Materials, 2019, 7(8): 1801415.

[26] Wang E L, Niu J B, Liang Y H, et al. Complete control of multichannel, angle-multiplexed, and arbitrary spatially varying polarization fields[J]. Advanced Optical Materials, 2020, 8(6): 1901674.

[27] Liang Y Y, Wei Z C, Guo J P, et al. Metalenses based on symmetric slab waveguide and c-TiO_2: efficient polarization-insensitive focusing at visible wavelengths[J]. Nanomaterials, 2018, 8(9): 699.

[28] Fan Q B, Liu M Z, Yang C, et al. A high numerical aperture, polarization-insensitive metalens for long-wavelength infrared imaging[J]. Applied Physics Letters, 2018, 113(20): 201104.

[29] Ozer A, Yilmaz N, Kocer H, et al. Polarization-insensitive beam splitters using all-dielectric phase gradient metasurfaces at visible wavelengths[J]. Optics Letters, 2018, 43(18): 4350-4353.

[30] Luo J, Xu P, Sun T T, et al. Tunable beam splitting and negative refraction in heterostructure with metamaterial[J]. Applied Physics A, 2011, 104(4): 1137-1142.

[31] Khorasaninejad M, Zhu A Y, Roques-Carmes C, et al. Polarization-insensitive metalenses at visible wavelengths[J]. Nano Letters, 2016, 16(11): 7229-7234.

[32] Ding F, Yang Y Q, Deshpande R A, et al. A review of gap-surface plasmon metasurfaces: fundamentals and applications[J]. Nanophotonics, 2018, 7(6): 1129-1156.

Design of Achromatic Polarization-Insensitive Metalens

Liang Yu[1], Xu Yuanyuan[1*], Zou Yang[2], Xue Shuangshuang[1], Liao Jingrong[3], Pan Wenyan[1], Wang Yawei[1]

[1] *School of Physics and Electronic Engineering, Jiangsu University, Zhenjiang, Jiangsu* 212013, *China*;

[2] *Jingjiang College, Jiangsu University, Zhenjiang, Jiangsu* 212013, *China*;

[3] *School of Mechanical Engineering, Jiangsu University, Zhenjiang, Jiangsu* 212013, *China*

Abstract

Objective The diffraction-limited phenomenon in optical imaging make the evanescent wave carrying high-order modes of the beam attenuate rapidly when it leaves the object surface, which results in low resolution and affects imaging quality. At the same time, the modulation mechanism from traditional optics makes an optical system highly integrated, which is still difficult. Owing to the miniaturization and flexible control of phase, amplitude, and polarization of the beam, metalenses have been widely used in a variety of highly compact and efficient devices. To overcome dispersion effect caused by the incident light with different frequencies passing through dielectric materials and to reduce the impact on the imaging effect of an optical system in the wideband spectrum, a metalens is designed herein, which achieves constant focus in the visible light band from 500 nm to 550 nm based on the titanium dioxide unit nanopillar. At the same time, to reduce the energy loss caused by the introduction of a polarizer in the traditional optical system, the achromatic metalens is introduced, which has also polarization-insensitive characteristics. The lens improves the imaging resolution of a multi-wavelength microscopy imaging system and has good applicability in the fields of digital cameras and optical instruments.

Methods Based on the phase compensation theory, the transmission phase method and the particle swarm optimization algorithm are used in this paper to design an achromatic metalens, and the first and higher derivative terms of the incident light phase information can make the incident light with different wavelengths arrive at the same time. In the same focal plane, to achieve this goal, the unit structure that meets this condition is selected. Usually, the geometric phase method is used for designing with polarization sensitivity. To satisfy the polarization insensitivity of the metalens on the basis of achromatic aberration and ensure both linearly polarized light and circularly polarized light to be incident, square nanopillars are selected as functional units here. After the structure of the unit has been determined, the selection of the unit with different widths and the design of the arrangement mode are studied in order to achieve the effective control of the deflection of the incident light beam with different wavelengths and achieve the correction effect of chromatic aberration. The width and height of a square nanopillar as well as the distance between the centers of adjacent nanopillars are optimized. The cross-sectional area of the square ranges from 0 to 1 to maximize the filling factor range and ensures that the polarization is not sensitive. The height of the square unit pillar is set as 600 nm to improve phase coverage. In actual manufacturing, due to the limited process level, the achievable shortest unit column width is 80 nm and the maximum width is the center distance of adjacent nanopillars. The Nyquist sampling criterion is followed to ensure the integrity of the beam information and ensure that the efficiency impact is low. The particle swarm optimization algorithm is used to select a structure, which achieves the achromatic effect to match the ideal phase value at each pixel, and the titanium dioxide nanopillars are scanned using the CST Microwave Studio electromagnetic simulation software to obtain the final superstructure with different unit nanopillar widths corresponding to the phases required for lens arrangement. To excite guided-mode resonances with different dispersion, the period of the unit column should be greater than the bandwidth of all transmitted wavelengths and smaller than the wavelength of incident light in free space to suppress higher-order diffraction. Therefore, the period of the unit column is 400 nm.

Results and Discussions Due to the dispersion of optical materials, the obtained images have chromatic aberration. The use of polarizers in traditional optical systems causes energy loss, and the overall device energy utilization rate is low. At present, most of the designed metalenses with an achromatic function in visible light and near-infrared light have polarization sensitivity. Therefore, this paper presents the design of an achromatic polarization-insensitive metalens based on the titanium dioxide unit nanopillar. In addition, the selected basic unit column is scanned using the CST Microwave Studio electromagnetic simulation software to make phases of unit

columns with different widths linearly propotortional to the incident light frequency (**Fig. 3**). At the same time, the particle swarm optimization algorithm is used to find the additional constant phase for adjusting the wavefront, and the optimal phase distribution is obtained, which is used for the metalens to achieve the achromatic effect. Compared with the phase distribution obtained without the particle swarm optimization algorithm, the obvious phase compensation improves the focusing efficiency without chromatic aberration (**Fig. 4**). By simulating the polarization-insensitive achromatic metalens designed in this paper, the achromatic effect is achieved at the focal length of 450 nm for the incident light with 500–550 nm wavelength, and it is compared with that of a dispersive metalens with the same numerical aperture (**Fig. 6**). The CST Microwave Studio electromagnetic simulation software is used to simulate the intensity of the reflected beam by the metalens. It is observed that the intensity of the reflected beam in the xoy plane exceeds 90% (**Fig. 7**). To verify the polarization insensitivity of the selected functional unit, the polarization angle is set between 0 and 90° with 9° as the step sweep parameter under the incidence of linear polarized light of a single nanopillar. Under different polarization states, the same diffraction efficiency of the incident light at different angles of incidence remains constant, and the diffraction efficiency increases with the increase of the wavelength. Therefore, the metalens designed in this paper effectively realizes the achromatic and polarization-insensitive characteristics.

Conclusions To summarize, this paper presents the use of titanium dioxide nanomaterials to design a reflective metalens under visible light. The chromatic aberration is successfully eliminated between 500 nm and 550 nm incident light, and the designed achromatic polarization-insensitive metalens is compared with a dispersive metalens with the same numerical aperture. It is a breakthrough in the limitation of traditional diffractive optics. To achieve achromatic effects, the achromatic polarization-insensitive metalens designed in this paper allows linearly polarized light and circularly polarized light with different chirality to be incident. Based on the design method of transmission phase theory and particle swarm optimization algorithm, this paper provides a reference for the field of metasurface device design, makes a contribution to the high integration of optical systems, and the designed achromatic polarization-insensitive metalens has a wide range of application in microscopic imaging and optical instruments.

Key words optical design; optical material; metalens; achromatic lens; polarization-insensitive; multi-wavelength; microscopic imaging

OCIS codes 220.4241; 220.3630; 260.2030; 260.5430